

Hybrid Membrane of Sulfonated Poly(aryl ether ketone sulfone) Modified by Molybdenum Clusters with Enhanced Proton Conductivity

Fang Ji, Fengyu Jiang, Hongwei Luo, Wen-Wen He,* Xu Han, Wangwang Shen, Menglong Liu, Tao Zhou, Jingmei Xu, Zhe Wang,* and Ya-Qian Lan*

Developing novel proton exchange membranes (PEMs) with low cost and superior performance to replace Nafion is of great significance. Polyoxometalate-doped sulfonated poly(aryl ether ketone sulfone) (SPAEEKS) allows for the amalgamation of the advantages in each constituent, thereby achieving an optimized performance for the hybrid PEMs. Herein, the hybrid membranes by introducing 2MeIm- $\{Mo_{132}\}$ into SPAEEKS are obtained. Excellent hydrophilic properties of 2MeIm- $\{Mo_{132}\}$ can help more water molecules be retained in the hybrid membrane, providing abundant carriers for proton transport and proton hopping sites to build successive hydrophilic channels, thus lowering the energy barrier, accelerating the proton migration, and significantly fostering the proton conductivity of hybrid membranes. Especially, SP-2MIMO $_{132}$ -5 exhibits an enhanced proton conductivity of 75 mS cm^{-1} at 80°C , which is 82.9% higher than pristine SPAEEKS membrane. Additionally, this membrane is suitable for application in proton exchange membrane fuel cells, and a maximum power density of 266.2 mW cm^{-2} can be achieved at 80°C , which far exceeds that of pristine SPAEEKS membrane (54.6 mW cm^{-2}). This work demonstrates that polyoxometalate-based clusters can serve as excellent proton conduction sites, opening up the choice of proton conduction carriers in hybrid membrane design and providing a novel idea to manufacture high-performance PEMs.

1. Introduction

With the large consumption of traditional fossil fuels, mankind is facing the great challenge of energy exhaustion and environmental crisis. Searching for sustainable and clean energy has become

a top priority.^[1,2] Proton exchange membrane fuel cells (PEMFCs) have already ensnared the attention of researchers, thanks to their noteworthy attributes, including elevated power density, rapid initiation, environmentally friendly emissions, and other outstanding qualities.^[3–5] As proton carriers as well as electron or neutral molecular barriers, proton exchange membranes (PEMs) have a significant influence on the durability and electrochemical performance of PEMFCs.^[6] At present, commercial Nafion has high conductivity and excellent stability, but their high fuel penetration, high humidity-dependent conductivity, complex manufacturing process, and high cost limit their further applications. Therefore, people cast their sights on the non-fluorinated PEM, such as polybenzimidazole (PBI), polyimide (PI), and sulfonated poly(aryl ether ketone sulfone) (SPAEEKS) to replace Nafion.^[7,8] Among them, SPAEEKS is a good alternative to Nafion owing to their cost-effectiveness, low methanol penetration, and high thermal stability. In SPAEEKS, a great proton

conductivity is usually achieved by high degree of sulfonation (DS), but high DS increases its molecular bulkiness, leading to excessive swelling.^[9] As a result, in order to obtain high proton conduction ability at low DS, modification of SPAEEKS is an urgent issue in the field of PEMs.^[10,11]

Polyoxometalates (POMs) are metal-oxygen cluster compounds formed by early-transition metal ions and oxygen atoms. It exhibits charming attributes such as modifiable structure, remarkable thermal stability and outstanding redox capabilities, and so forth.^[12] Moreover, POMs are commonly used as high proton conductors owing to the advantages of oxygen enrichment on the surface, strong acidity, and commendable electrochemical stability.^[13] Recently, researchers have shown an increased interest in incorporating POMs into polymer membrane matrix as an excellent proton conductors. In 2018, Wu synthesized a proton-conducting composite membrane $\text{rGO-P}_2\text{W}_{16}\text{V}_2@\text{SPEEK}$, exhibiting excellent proton conductivity of $7.90 \times 10^{-2} \text{ S cm}^{-1}$ at 50°C .^[14] In 2020, Zang reported a hybrid membrane (Nafion-Bi $_{12}$ -3%) fabricated by doping $\{H_6Bi_{12}O_{16}\}$ clusters into Nafion. The proton conductivity of Nafion-Bi $_{12}$ -3% has been promoted to

F. Ji, F. Jiang, H. Luo, W.-W. He, X. Han, W. Shen, M. Liu, T. Zhou, J. Xu, Z. Wang

School of Chemistry and Life Science
Advanced Institute of Materials Science
Changchun University of Technology
Changchun 130012, P. R. China

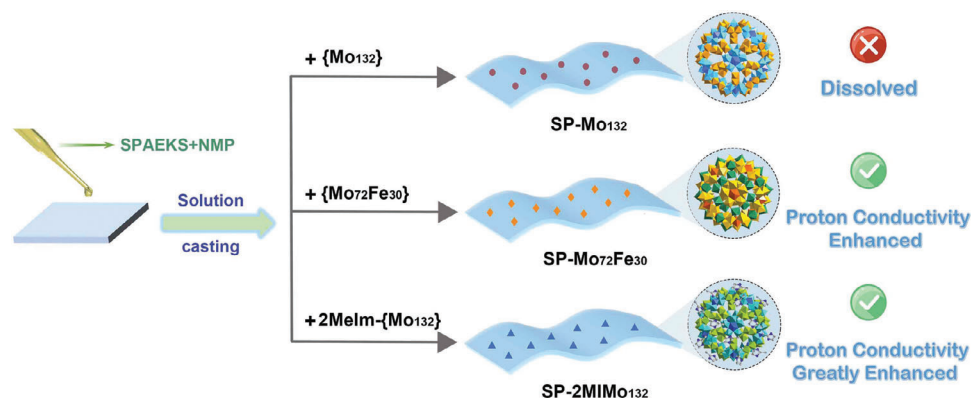
E-mail: heww@ccut.edu.cn; wangzhe@ccut.edu.cn

Y.-Q. Lan

School of Chemistry
South China Normal University
Guangzhou 510006, P. R. China
E-mail: yqlan@m.scnu.edu.cn

The ORCID identification number(s) for the author(s) of this article can be found under <https://doi.org/10.1002/sml.202312209>

DOI: 10.1002/sml.202312209



Scheme 1. Schematic of SPAEKS hybrid membranes modified by molybdenum clusters.

386 mS cm⁻¹ at 80 °C.^[15] In 2022, Li introduced GSiW₁₁ (SiW₁₁ grafted by polyethylene glycol) into Nafion, obtaining a hybrid membrane (GSiW₁₁-Nf-3%) that reached ultrahigh conductivity of 226 mS cm⁻¹ at 80 °C.^[16] All these proved that POMs are excellent inorganic fillers to PEMs.

Molybdenum clusters are extraordinary candidates for proton conductors. Their prominent performance is summarized as the following reasons. First, the oxygen-enriched surfaces of molybdenum clusters can provide sufficient proton transfer sites, following the Grotthuss mechanism. Second, the presence of cavities and pore structures of molybdenum clusters allow discrete water molecules to enter and exit freely, facilitating proton transport via the vehicle mechanism.^[17,18] Based on the aforementioned advantages, molybdenum clusters have gained increasing attention as a research focus in the field of proton conduction. In 2020, Lan presented a 240-nuclearity giant polymolybdate cage {Mo₂₄₀}, which exhibited a superior proton conductivity of 1.03 × 10⁻¹ S cm⁻¹ at 80 °C.^[19] In 2021, Kong synthesized a 3D molybdenum cluster 3D-{Mo₁₅₄}_n, revealing the conductivity of 1.1 × 10⁻² S cm⁻¹ at 22 °C.^[20] These examples confirmed the great potential of molybdenum clusters as proton conductors.

In this work, molybdenum clusters have been first introduced into SPAEKS to construct hybrid membranes (**Scheme 1**). First of all, we introduced {Mo₁₃₂} into SPAEKS to prepare hybrid membranes (SP-Mo₁₃₂). It was a pity that the highly hydrophilic of {Mo₁₃₂} resulted in a serious leakage of POMs from the SPAEKS matrix. Next, we obtained membranes by hybridizing SPAEKS with {Mo₇₂Fe₃₀} (30 Mo atoms replaced by 30 Fe atoms), named as SP-Mo₇₂Fe₃₀. Notably, we found that the water solubility of {Mo₇₂Fe₃₀} had been greatly reduced.^[21] Meanwhile, SP-Mo₇₂Fe₃₀-3 can show excellent proton conductivity of 66 mS cm⁻¹ at 80 °C. To further improve the proton conductivity, we introduced N-containing ligands (2-methylimidazole) into the system. {Mo₁₃₂} modified by 2-methylimidazole ligand (2MeIm-{Mo₁₃₂}) had been incorporated into SPAEKS, named as SP-2MIMO₁₃₂. The 2-methylimidazole ligand can build hydrogen bonds with the sulfonic acid group of SPAEKS. This host-guest interaction can greatly reduce the dissolution of the POMs, furthermore, providing extra transfer sites and obtaining extended hydrogen bond network for proton transport.^[22,23] Particularly, the hybrid membrane (SP-2MIMO₁₃₂-5) displayed a wonderful conductivity

of 75 mS cm⁻¹ at 80 °C. This study indicates that the introduction of POMs cluster is a feasible strategy to enhance the proton conduction of hybrid membranes.

2. Results and Discussion

2.1. Characterization of {Mo₇₂Fe₃₀} and 2MeIm-{Mo₁₃₂}

The polyhedral structures of {Mo₇₂Fe₃₀} and 2MeIm-{Mo₁₃₂} are shown in **Figure 1**. {Mo₇₂Fe₃₀} is an icosahedral cluster consisting of 12 [(Mo^{VI})Mo₅^{VI}O₂₁]⁶⁻ second building units (SBUs) and 30 {Fe^{III}(H₂O)} SBUs, containing cavities with a diameter of 2.5 nm. In addition, there are 91 ligand water molecules and 150 free water molecules in the structure.^[24] 2MeIm-{Mo₁₃₂} is an icosahedral cluster consisting of 12 {(Mo^{VI}O₇)(Mo^{VI}O₆)₅} SBUs and 30 {Mo₂^VO₄(OOCCH₃)⁺} SBUs. There are 72 coordination water molecules and up to 190 free water molecules in the structure, and it has a cavity that is 2 nm in diameter. The presence of these coordination water and free water will provide continuous proton transport sites for subsequent proton conduction. Furthermore, the structure of 2MeIm-{Mo₁₃₂} has 20 hexagonal windows which are larger than the diameter of the guest molecule, providing enough space and an easier route for proton transfer.^[25] Besides, there are 2-methylimidazole ligands both inside and outside the hollow spherical cluster. Nitrogen-containing ligands can provide more additional transport sites and carriers for proton conduction, resulting in a significant enhancement in proton conductivity.

Figure S1a (Supporting Information) depicts the FT-IR spectra of POMs. The stretching vibration of the C=C bond and the bending vibration of the C-H bond, respectively, account for the peaks at 1571 and 1151 cm⁻¹. The characteristic peaks of the acetic acid group are located between 1550 and 1400 cm⁻¹, and the weak peaks at 940 cm⁻¹ can be ascribed to the stretching vibration of Mo=O bond. In addition, strong peaks ≈580 and 798 cm⁻¹ are derived from the bending and asymmetric stretching vibrations of the Mo-O-Mo bond, respectively. The weak peaks ≈650 cm⁻¹ can be assigned to Fe-O bond.^[26,27] The presence of these characteristic peaks demonstrates that {Mo₇₂Fe₃₀} and 2MeIm-{Mo₁₃₂} have been synthesized successfully. PXRD patterns of the prepared {Mo₇₂Fe₃₀} and 2MeIm-{Mo₁₃₂} are consistent with the simulated ones (Figure S2, Supporting

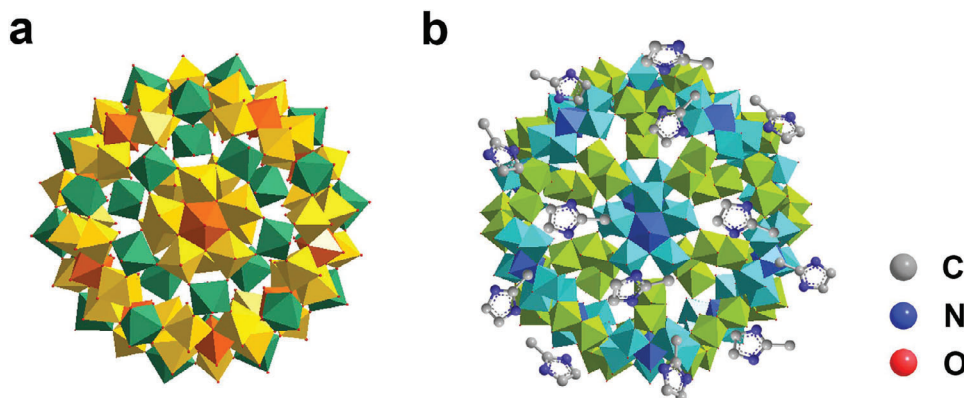


Figure 1. a) Polyhedral structure of $\{\text{Mo}_{72}\text{Fe}_{30}\}$ (orange polyhedron: $\{\text{MoO}_7\}$, yellow polyhedron: $\{\text{MoO}_6\}$, dark green polyhedron: $\{\text{FeO}_6\}$). b) Polyhedral structure of 2MeIm- $\{\text{Mo}_{132}\}$ (dark blue polyhedron: $\{\text{MoO}_7\}$, cyan and light green polyhedron: $\{\text{MoO}_6\}$).

Information), respectively, further illustrating that these two compounds have been successfully synthesized and both of them have high phase purity.^[28]

TGA tests were carried out to explore the thermal stability of two compounds. Figure S1b (Supporting Information) depicts the weight loss of $\{\text{Mo}_{72}\text{Fe}_{30}\}$. The weight loss at 100 °C in the first stage is related to the loss of coordination between water and free water. The second stage at ≈ 290 °C is ascribed to the dissociation of acetic acid in $\{\text{Mo}_{72}\text{Fe}_{30}\}$. The third stage at about 700 °C is attributed to the collapse of the POM skeleton. The TGA curve of 2MeIm- $\{\text{Mo}_{132}\}$ mainly shows two stages of degradation and it can be stable up to 200 °C (Figure S1b, Supporting Information). The results of TGA analysis imply that these two compounds have good stability within the allowable temperature of the cells.

2.2. Characterization of SPAEKS

As illustrated in Figure 2, the signal at δ 8.22 ppm comes from hydrogen in the benzene ring with $-\text{SO}_3\text{Na}$. The chemical signal from δ 6.87 to 8.33 ppm comes from hydrogen in the benzene ring, and the signal from δ 1.54 to 1.71 ppm corresponds to the hydrogen of $-\text{CH}_3$. The fact that aforementioned results are in line with those mentioned in earlier literature,^[29] which demonstrated that the SPAEKS polymer was successfully synthesized.

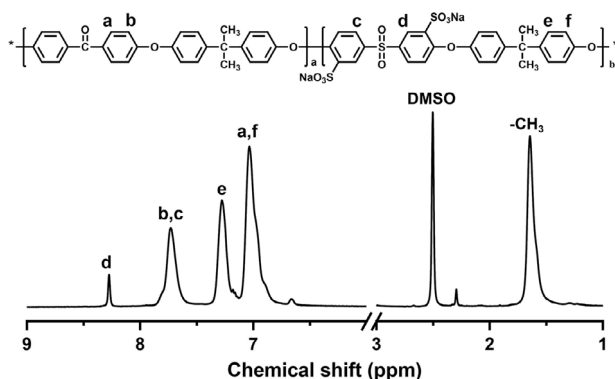


Figure 2. ^1H NMR spectra of SPAEKS.

2.3. Characterization of the Membranes

ATR-FT-IR was used to verify the structure of pristine membranes and hybrid membranes (Figure 3a,c). The peaks of $-\text{SO}_3\text{H}$ group show up at 1082 and 1227 cm^{-1} . They are asymmetric stretching vibration and symmetric stretching vibration of $\text{O}=\text{S}=\text{O}$, respectively. The peaks of benzene ring are 1592 and 1498 cm^{-1} , respectively. The peak at 1650 cm^{-1} is derived from the carbonyl peak in SPAEKS.^[30] The above further confirms that SPAEKS is successfully synthesized. Because of the relatively low loading amounts, there are no characteristic peaks of $\{\text{Mo}_{72}\text{Fe}_{30}\}$ and 2MeIm- $\{\text{Mo}_{132}\}$ in the infrared spectra.

TGA curves of all the membranes are depicted in Figure 3b,d. Pristine membrane and hybrid membranes exhibit three-step weightlessness over the entire temperature range (30–800 °C). The loss of water results in the first weightlessness that occurs at 200 °C. The second weight loss occurs at 300 °C owing to thermal decomposition of the sulfonic acid group. The third weight loss that appears at 400 °C was attributed to the thermal oxidation of the backbone.^[31] Overall, all hybrid membranes show better thermal stabilities, implying that the introduction of $\{\text{Mo}_{72}\text{Fe}_{30}\}$ and 2MeIm- $\{\text{Mo}_{132}\}$ help to improve the heat endurance of the hybrid PEMs.

2.4. Morphology Characterizations of the Membranes

The transparency and flexibility of SP- $\text{Mo}_{72}\text{Fe}_{30}$ -3 and SP-2MIMO₁₃₂-5 are demonstrated in Figure 4, respectively. Obviously, the transparency of the hybrid membranes is good, and there is no accumulation of inorganic dopants, indicating that SPAEKS is compatible with $\{\text{Mo}_{72}\text{Fe}_{30}\}$ and 2MeIm- $\{\text{Mo}_{132}\}$. Additionally, hybrid membranes can be folded into any shape without breaking, revealing that the POMs-doped SPAEKS membranes have good mechanical properties and can meet the practical application of PEMFCs.

The micromorphology of pristine SPAEKS and hybrid membranes is observed by SEM. As shown in Figure 5a,e, the cross sections of pristine SPAEKS membranes are uniform and dense. It can be seen from Figure 5b–d and Figure 5f–h that with the increase of $\{\text{Mo}_{72}\text{Fe}_{30}\}$ and 2MeIm- $\{\text{Mo}_{132}\}$, the cross

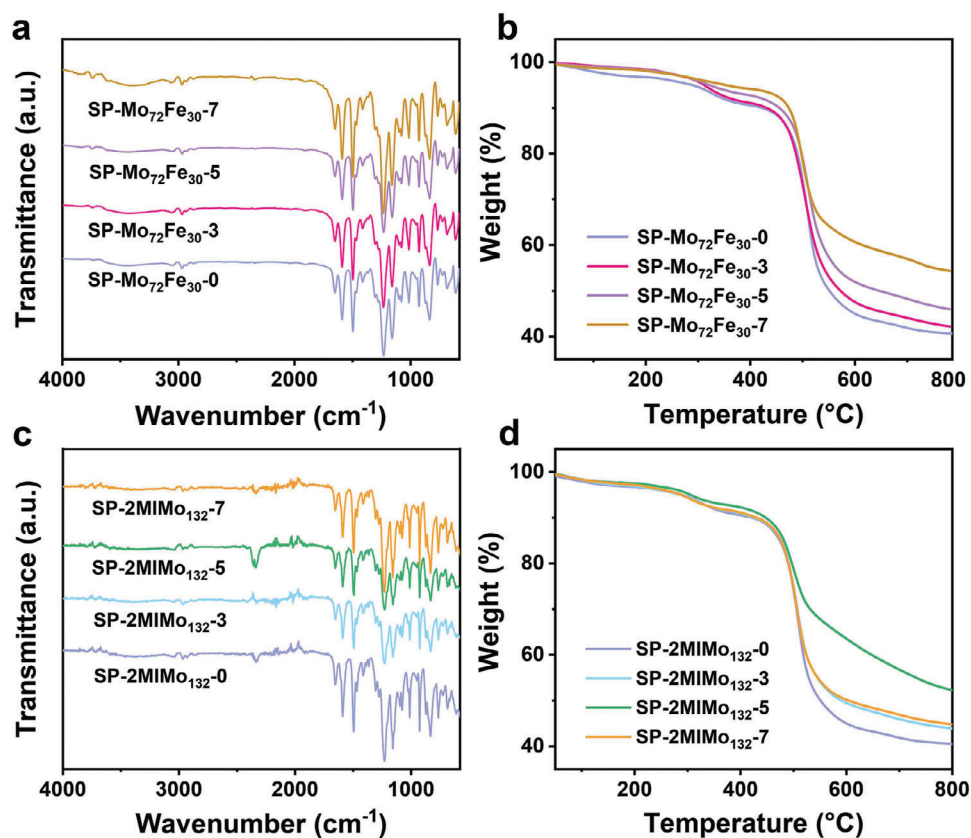


Figure 3. a) ATR-FT-IR spectra and b) TGA curves of SP-Mo₇₂Fe_{30-x} (x = 0, 3, 5, 7). c) ATR-FT-IR spectra and d) TGA curves of SP-2MIMO_{132-y} (y = 0, 3, 5, 7).



Figure 4. The transparency and flexibility of membranes. a,b): SP-2MIMO₁₃₂₋₅; c,d): SP-Mo₇₂Fe₃₀₋₃.

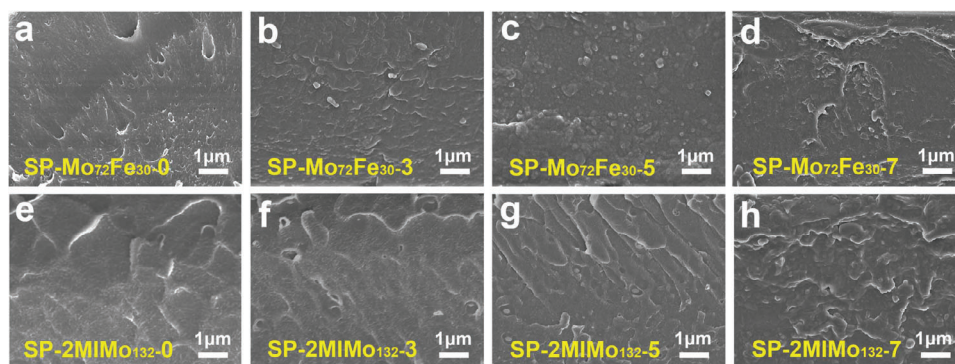


Figure 5. SEM images of the cross-section morphology. a–d): SP-Mo₇₂Fe_{30-x} (x = 0, 3, 5, 7), e–h): SP-2MIMO_{132-y} (y = 0, 3, 5, 7).

sections of the hybrid membranes become rough gradually, which proves that POMs have been successfully introduced into the SPAEKS membranes. In Figure 5d,h, as the load increased, it can be observed that some particle aggregations and large defects appeared in the membranes. This is probably because too much POMs have a bad influence to the compatibility of the polymers, destroying the dense structure of the membranes. The EDS mapping analysis was performed. As can be seen from Figure 6a, the elements of Mo and Fe are uniformly distributed in SP-Mo₇₂Fe₃₀₋₃, demonstrating the successful introduction of {Mo₇₂Fe₃₀} into SPAEKS and its uniform dispersion. As shown in Figure 6b, the elements of Mo and N are evenly distributed in SP-2MIMO₁₃₂₋₅, which proves that 2MeIm- $\{Mo_{132}\}$ is successfully introduced into SPAEKS and evenly dispersed. Additionally, XRD of pristine and hybrid membranes was also performed. As shown in Figure S3 (Supporting Information), no crystalline characteristic peaks of POMs are observed in these membranes, indicating that molybdenum clusters are homogeneously dispersed among the polymer chains without any aggregation. This is consistent with the SEM and EDS results.

2.5. Hydrophilicity, Water Uptake (WU), and Swelling Ratio (SR) of the membranes

Excellent hydrophilicity is an important prerequisite for high proton conductivity. In comparison to pristine membranes, hybrid membranes' water contact angles are smaller, among which SP-Mo₇₂Fe₃₀₋₃ and SP-2MIMO₁₃₂₋₅ are the smallest in the same series of hybrid membranes (Figure 7c,f). In other words, when the addition amount of {Mo₇₂Fe₃₀} and 2MeIm- $\{Mo_{132}\}$ reached 3 and 5 wt%, respectively, the hydrophilicity of the hybrid membranes is the best. This proves that POMs play a critical role in enhancing the hydrophilicity of hybrid membranes. A large amount of bound water in molybdenum cluster structure endows the membrane with good hydrophilicity. In addition, the porous structure of molybdenum cluster has a certain water storage capacity, which also contributes to the attraction of water molecules.^[32,33] Consequently, the introduction of molybdenum cluster increases the water-adsorbing ability of the membranes, which also assists proton transport.

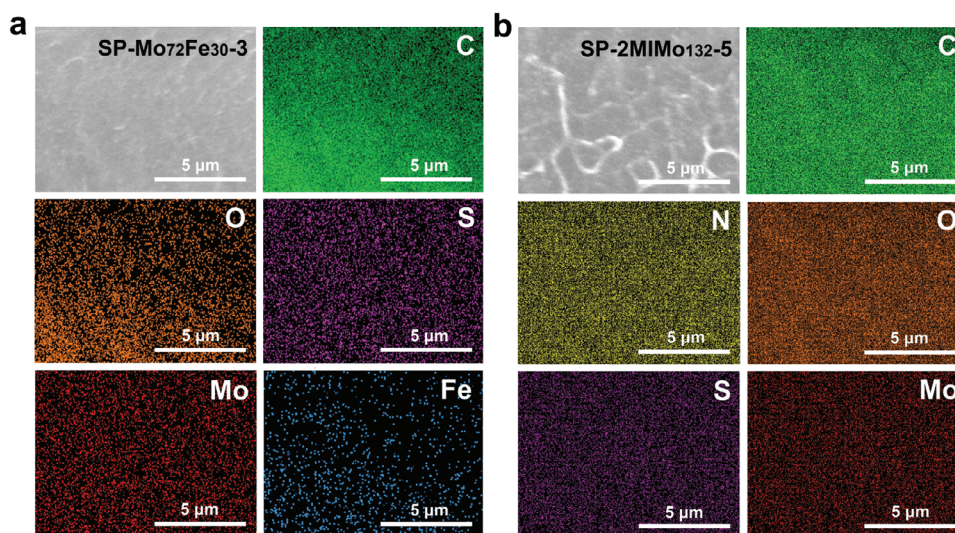


Figure 6. a) Cross-section morphology and elemental distribution mappings of C, O, S, Mo, Fe in SP-Mo₇₂Fe₃₀₋₃. b) Cross-section morphology and elemental distribution mappings of C, N, O, S, Mo in SP-2MIMO₁₃₂₋₅.

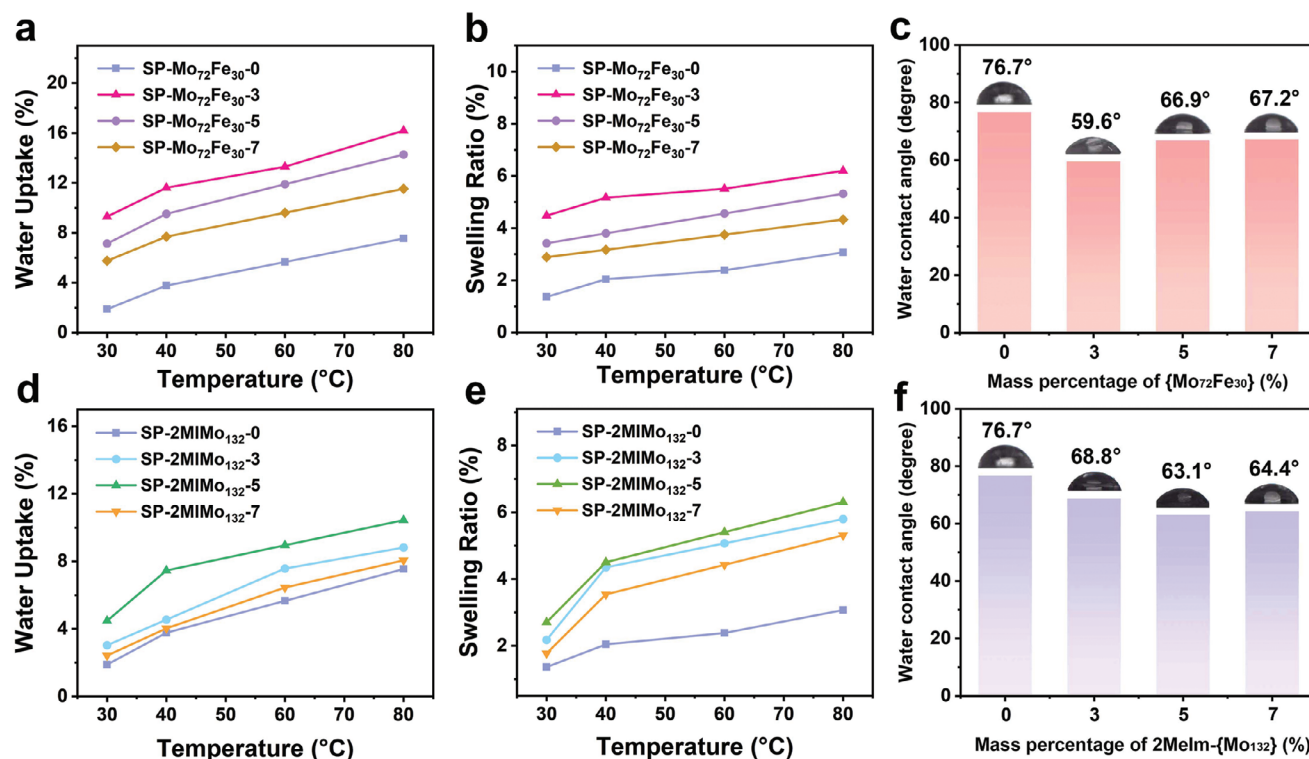


Figure 7. a) Water uptake, b) swelling ratio, and c) water contact angles of SP-Mo₇₂Fe_{30-x} (x = 0, 3, 5, 7). d) Water uptake, e) swelling ratio, and f) water contact angles of SP-2MIMO_{132-y} (y = 0, 3, 5, 7).

Water uptake (WU) and swelling ratio (SR) are two indispensable elements to measure the dimensional stability of PEMs.^[34] The WU of every membrane increases corresponding to temperature. Compared to pristine membranes, hybrid membranes manifest higher WU values, which SP-Mo₇₂Fe₃₀₋₃ and SP-2MIMO₁₃₂₋₅ reaches a maximum, respectively (Figure 7a,d). The results are in accord with the water contact angle test results. These reveal that the proper doping of hydrophilic compound {Mo₇₂Fe₃₀} and 2Melm-{Mo₁₃₂} help to construct a hydrogen bond network and improve the hydrophilicity of hybrid membranes. As the temperature rises, the movement of backbone is strengthened, and the large molecular chain gap allows more free water molecules to enter, so WU and SR of the hybrid membranes augment accordingly. However, when a higher content of POMs is introduced, the gap between the polymer molecular chains will be occupied,

thereby preventing the free movement of water molecules, leading to a decreased WU.^[32] In addition, there is only a slight increase of SR in every membrane (Figure 7b,e), manifesting that the membranes have excellent dimensional stability.

2.6. Mechanical Properties of the Membranes

The mechanical properties of the membrane directly affect the stable operation of batteries.^[35] By analyzing the values from Table 1, it is possible to deduce that compared with pristine membranes, the tensile strength and Young's modulus of all hybrid membranes have been improved. The tensile strength of SP-Mo₇₂Fe₃₀₋₃ and SP-2MIMO₁₃₂₋₅ reached the highest values, which were 38.62 and 26.34 MPa, respectively. The

Table 1. Mechanical properties of the pristine membrane and hybrid membranes.

Sample name	Young's modulus [GPa]	Tensile strength [MPa]	Elongation-at-break [%]	Oxidative stability	IEC [mmol g ⁻¹]	E _a [kJ mol ⁻¹]	λ [80 °C]
SP-M-0	1.05 ± 0.0166	22.37 ± 1.79	8.30 ± 1.35	98.31%	0.65	13.48	6.45
SP-Mo ₇₂ Fe ₃₀₋₃	1.57 ± 0.0268	38.62 ± 2.07	14.80 ± 1.84	98.38%	0.70	13.30	12.85
SP-Mo ₇₂ Fe ₃₀₋₅	1.52 ± 0.0439	35.66 ± 1.45	9.45 ± 3.78	95.74%	0.67	11.97	11.79
SP-Mo ₇₂ Fe ₃₀₋₇	1.50 ± 0.0175	29.73 ± 3.92	8.60 ± 2.56	98.31%	0.66	13.05	9.69
SP-2MIMO ₁₃₂₋₃	1.06 ± 0.0258	24.47 ± 0.43	12.40 ± 3.11	98.88%	0.72	12.88	6.80
SP-2MIMO ₁₃₂₋₅	1.07 ± 0.0937	26.34 ± 3.33	14.57 ± 0.52	99.43%	0.75	12.77	7.74
SP-2MIMO ₁₃₂₋₇	1.06 ± 0.0626	25.70 ± 1.06	25.13 ± 3.14	98.85%	0.68	12.85	6.58

(M represent Mo₇₂Fe₃₀ and 2MIMO₁₃₂)

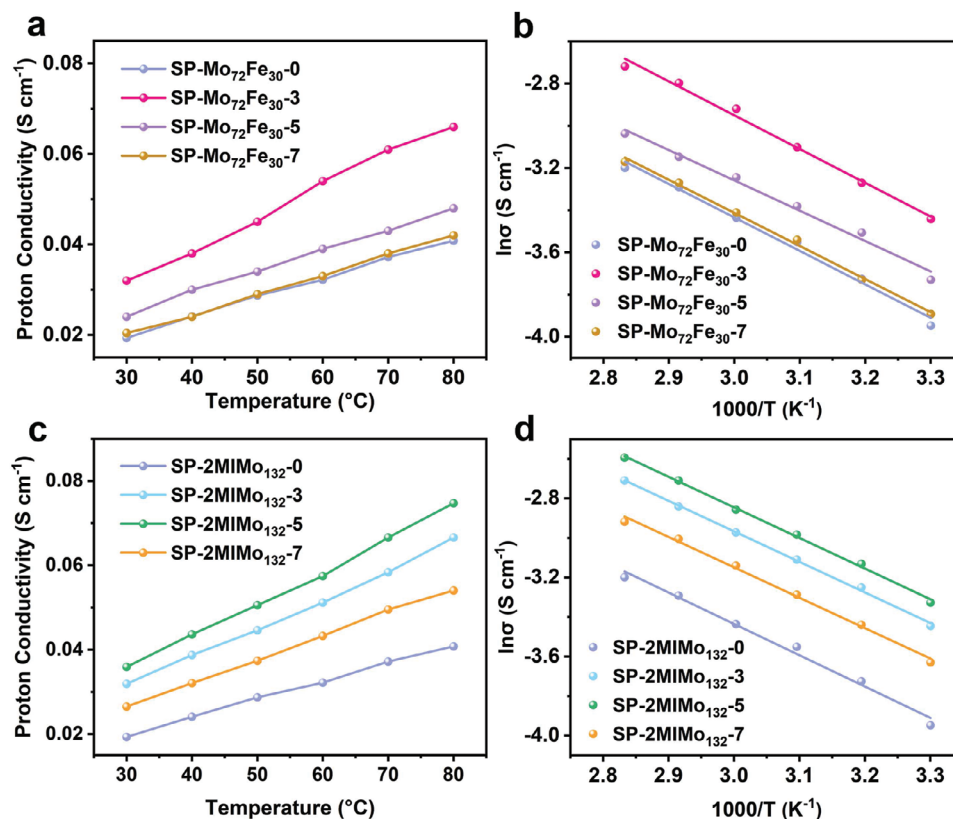


Figure 8. a) Proton conductivity and b) Arrhenius plot of SP-Mo₇₂Fe_{30-x} (x = 0, 3, 5, 7). c) Proton conductivity and d) Arrhenius plot of and SP-2MIMO_{132-y} (y = 0, 3, 5, 7) at different temperatures.

electrostatic interaction between guest molecule POMs and sulfonic acid groups may be contributing to this improvement in mechanical characteristics, which provide sufficient interaction force for the rigidity of the membranes.^[36] When the excessive POMs (more than 10 wt%) are introduced into the polymer matrix, the electrostatic interaction between SPAEKS and POMs will be weakened, and the compatibility between the two will be greatly reduced, which will lead to the deterioration of mechanical properties (Table S1, Supporting Information).

2.7. Proton Conductivity and Activation Energy of the Membranes

The primary factor to consider when assessing a PEM is its proton conductivity.^[37] The proton conductivities of membranes are investigated at various temperatures in Figure 8a,c. At the same temperature, hybrid membranes exhibit higher proton conductivities than that of pristine SPAEKS. Among which {Mo₇₂Fe₃₀} series membranes display the highest proton conductivity at 3 wt% doping content (up to 66 mS cm⁻¹ at 80 °C). While the 2MeIm-{Mo₁₃₂} series membranes show the highest proton conductivity at 5 wt% doping content (up to 75 mS cm⁻¹ at 80 °C). These results are in agreement with those obtained by water uptake. The above reveals that {Mo₇₂Fe₃₀} and 2MeIm-{Mo₁₃₂} contribute greatly to the increase of proton conductivity.^[38]

Taking SP-2MIMO₁₃₂₋₅ as an example, the stable existence of the hybrid membranes can be ascribed to the electrostatic interaction between the sulfonic acid groups and the nitrogen atoms in 2MeIm-{Mo₁₃₂}. The main reasons for the significant increase in proton conductivity of SP-2MIMO₁₃₂₋₅ are summarized as follows: the large number of hydrophilic sites on the surface of 2MeIm-{Mo₁₃₂} and its inherent cavities in the hollow structure assist in absorbing more water as proton carriers. Both the H₃O⁺ and the protonated 2MeIm in the system can meanwhile act as proton carriers participate in the formation of proton conduction pathways and enhance the proton transfer ability by the vehicle mechanism.^[39,40] The interaction of hydrogen bonding between POMs and -SO₃H provides continuous proton transport channels for proton conduction via the Grotthuss mechanism. In addition, the 2-MeIm unit has two N atoms: one N contains an intrinsic proton H as a proton source, while the other readily accepts H to form N-H...O hydrogen bonds, offering extra proton transfer sites and reducing the energy barrier of the proton transport process.^[41] More importantly, the electrostatic interaction between -SO₃H and N-H (2MeIm) promotes the dissociation of protons, further lowering the barrier for proton transfer and facilitating proton conduction.^[42-44] To sum up, the introduction of 2MeIm-{Mo₁₃₂} increases the number of proton carriers and the density of proton hopping sites, accelerating the proton migration and effectively enhancing the proton conductivity of hybrid PEMs under the synergistic effect of the two mechanisms (Figure 9).

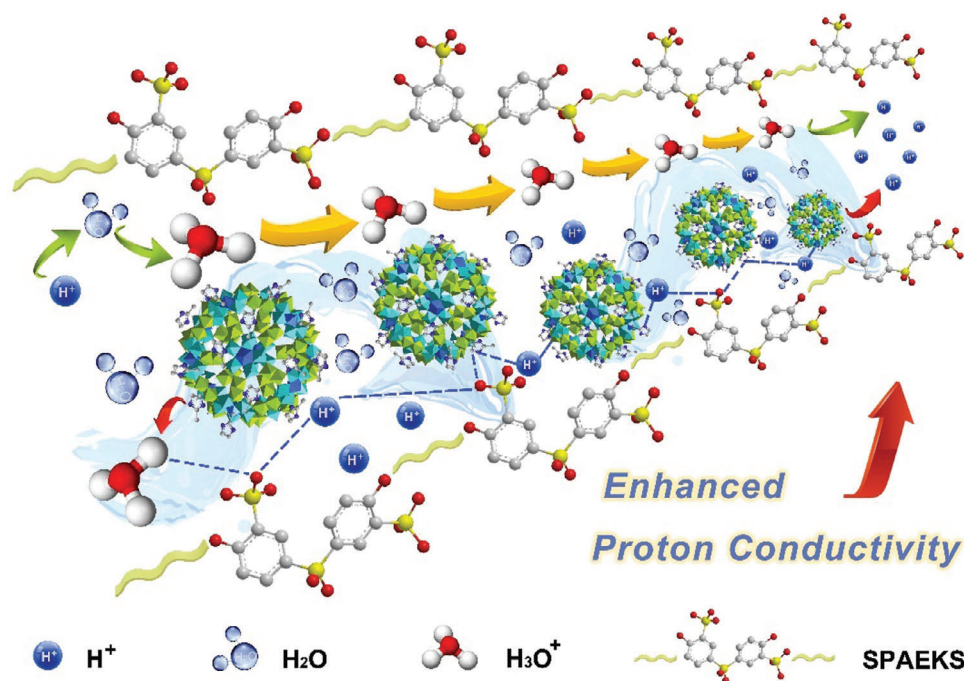


Figure 9. Schematic illustration of the proton transport of hybrid membranes SP-2MIMO₁₃₂₋₅.

2.8. Oxidative Stability and Ion Exchange Capacity (IEC) of the Membranes

The oxidation stability values of membranes are shown in Table 1. The residual weight percentages of all membranes were between 95.74% and 99.43%. Among them, the antioxidant stability of 2MeIm- $\{Mo_{132}\}$ series membranes is higher than that of $\{Mo_{72}Fe_{30}\}$ series, which may be due to the presence of nitrogen-containing ligands. The oxidation stability of hybrid membrane SP-2MIMO₁₃₂₋₅ is very high, exceeding that of most hybrid membranes reported. This excellent oxidation stability could be ascribed to the existence of nitrogen atoms in 2MeIm which can react with ferrous ions in the Fenton reagent to reduce the activity of hydroxyl radicals, thus raising the oxidation stability of the membranes.^[45]

The IEC values of the series of membrane materials are listed in Table 1. The hybrid membranes exhibited higher IEC values than pristine ones, and IEC peaks of SP- $Mo_{72}Fe_{30}$ -3 and SP-2MIMO₁₃₂₋₅ are as follows: 0.70, and 0.75 mmol g⁻¹. Although the degree of sulfonation of SPAEKS is relatively low (DS = 30%), $\{Mo_{72}Fe_{30}\}$ and 2MeIm- $\{Mo_{132}\}$ can dissociate a large number of protons, compensating for the reduction of IEC caused by the lower concentration of sulfonic acid group. As expected, benefiting from the protons generated from 2-MeIm, SP-2MIMO₁₃₂₋₅ reaches the highest IEC value.^[46,47]

2.9. Fuel Cell Performance of SPAEKS and Hybrid Membranes

The electrochemical performance of PEMs is critical in their practical applications. As illustrated in Figure 10, the polarization curves and power density curves of SPAEKS, SP- $Mo_{72}Fe_{30}$ -3, and SP-2MIMO₁₃₂₋₅ are evaluated. The open circuit voltages of

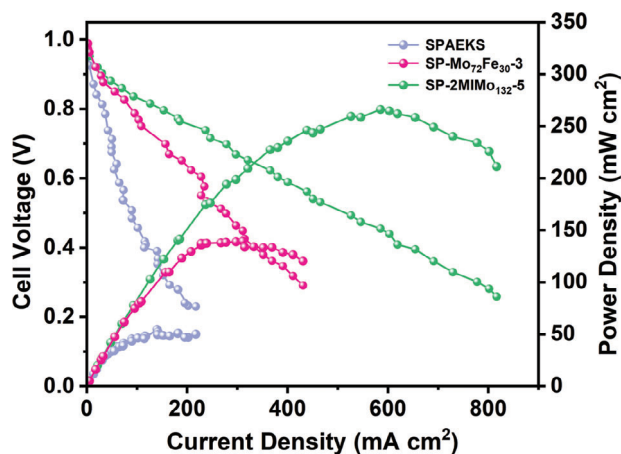


Figure 10. Single H₂/O₂ cell performance of SPAEKS, SP- $Mo_{72}Fe_{30}$ -3, and SP-2MIMO₁₃₂₋₅ operated at 80 °C.

the three membranes are both above 0.95 V, manifesting their superior gas barrier property and remarkable electrode activity. The maximum power density of SP- $Mo_{72}Fe_{30}$ -3 and SP-2MIMO₁₃₂₋₅ is 139.4, and 266.2 mW cm⁻², which is much higher than 54.6 mW cm⁻² of pristine SPAEKS at the exact same test conditions. The results demonstrate that these molybdenum cluster-doped hybrid membranes have excellent prospects for use in PEMFCs.

3. Conclusion

In this work, a strategy of introducing molybdenum clusters ($\{Mo_{72}Fe_{30}\}$ and 2MeIm- $\{Mo_{132}\}$) into SPAEKS to construct hybrid membranes is proposed. According to the findings, the

hybridization effect of 2MeIm-Mo₁₃₂ is preferable. SP-2MIMO₁₃₂-5 possesses the highest proton conductivity of 75 mS cm⁻¹ at 80 °C and a peak power density of 266.2 mW cm⁻², which exhibits great potential to be applied in fuel cells. The hydrophilic properties of 2MeIm-{Mo₁₃₂} can help the hybrid membrane absorb more water molecules to act as additional proton carriers. Meanwhile, oxygen atoms in POMs and nitrogen atoms in ligands contribute to a large number of proton hopping sites. Consequently, the proton jump energy barrier has been lowered and the proton conductivity has been effectively increased. In addition, the strong interaction between POMs and the main chain endows the hybrid membranes with excellent oxidation stability, and improved mechanical and dimensional stabilities. In summary, this study indicates that POMs have a positive effect on elevating the comprehensive performance of PEMs and offers a general strategy for developing POMs as promising proton conduction carriers for PEMs.

Supporting Information

Supporting Information is available from the Wiley Online Library or from the author.

Acknowledgements

F.J. and F.J. contributed equally to this work. This work was financially supported by the National Natural Science Foundation of China (No. 22271022), and the Science and Technology Development Planning of Jilin Province (No. YDZJ202201ZYTS342). This work was also supported by the China Scholarship Council (CSC No. 201802335014).

Conflict of Interest

The authors declare no conflict of interest.

Data Availability Statement

The data that support the findings of this study are available from the corresponding author upon reasonable request.

Keywords

molybdenum clusters, polyoxometalates, proton conductivity, proton exchange membrane, sulfonated poly(aryl ether ketone sulfone)

Received: December 27, 2023

Revised: March 6, 2024

Published online:

- [1] J. Zhou, J. Cao, Y. Zhang, J. Liu, J. Chen, M. Li, W. Wang, X. Liu, *Renew. Sustain. Energy Rev.* **2021**, *138*, 110660.
- [2] S. Ahmad, T. Nawaz, A. Ali, M. F. Orhan, A. Samreen, A. M. Kannan, *Int. J. Hydrogen Energy* **2022**, *47*, 19086.
- [3] B. Lv, K. Geng, H. Yin, C. Yang, J. Hao, Z. Luan, Z. Huang, X. Qin, W. Song, N. Li, Z. Shao, *J. Membr. Sci.* **2021**, *639*, 119760.

- [4] X. Sun, J.-H. Song, H.-Q. Ren, X.-Y. Liu, X.-W. Qu, Y. Feng, Z.-Q. Jiang, H.-L. Ding, *Electrochim. Acta* **2020**, *331*, 135235.
- [5] B. Zhang, Y. Cao, Z. Li, H. Wu, Y. Yin, L. Cao, X. He, Z. Jiang, *Electrochim. Acta* **2017**, *240*, 186.
- [6] Y. Lu, Y. Liu, N. Li, Z. Hu, S. Chen, *J. Membr. Sci.* **2020**, *601*, 117908.
- [7] H. Guo, Z. Li, H. Pei, P. Sun, L. Zhang, P. Li, X. Yin, *J. Membr. Sci.* **2022**, *644*, 120092.
- [8] A. Ghorai, S. Banerjee, *Prog. Polym. Sci.* **2023**, *138*, 101646.
- [9] S. Zhong, C. Liu, Z. Dou, X. Li, C. Zhao, T. Fu, H. Na, *J. Membr. Sci.* **2006**, *285*, 404.
- [10] M. Xu, H. Xue, Q. Wang, L. Jia, *Int. J. Hydrogen Energy* **2021**, *46*, 31727.
- [11] M. Ju, L. Meng, J. Xu, X. Chen, J. Yu, Z. Wang, *J. Ind. Eng. Chem.* **2023**, *123*, 342.
- [12] Y. Zhang, Y. Liu, D. Wang, J. Liu, J. Zhao, L. Chen, *Polyoxometalates* **2023**, *2*, 9140017.
- [13] M. R. Horn, A. Singh, S. Alomari, S. Goberna-Ferrón, R. Benages-Vilau, N. Chodankar, N. Motta, K. Ostrikov, J. Macleod, P. Sonar, P. Gomez-Romero, D. Dubal, *Energy Environ. Sci.* **2021**, *14*, 1652.
- [14] H. Wu, X. Wu, Q. Wu, W. Yan, *Compos. Sci. Technol.* **2018**, *162*, 1.
- [15] B. Liu, B. Hu, J. Du, D. Cheng, H. Y. Zang, X. Ge, H. Tan, Y. Wang, X. Duan, Z. Jin, W. Zhang, Y. Li, Z. Su, *Angew. Chem., Int. Ed.* **2021**, *60*, 6076.
- [16] H. He, Y. Zhu, T. Li, S. Song, L. Zhai, X. Li, L. Wu, H. Li, *ACS Nano* **2022**, *16*, 19240.
- [17] C. Wang, T. Su, H.-Y. Zang, Z.-M. Su, *Mater. Chem. Front.* **2023**, *7*, 1912.
- [18] J.-C. Liu, J.-W. Zhao, C. Streb, Y.-F. Song, *Coord. Chem. Rev.* **2022**, *471*, 214734.
- [19] J. Lin, N. Li, S. Yang, M. Jia, J. Liu, X. M. Li, L. An, Q. Tian, L. Z. Dong, Y. Q. Lan, *J. Am. Chem. Soc.* **2020**, *142*, 13982.
- [20] H.-Y. Wang, S.-R. Li, X. Wang, L.-S. Long, X.-J. Kong, L.-S. Zheng, *Sci. Chi. Chem.* **2021**, *64*, 959.
- [21] T. Liu, B. Imber, E. Diemann, G. Liu, K. Cokleski, H. Li, Z. Chen, A. Müller, *J. Am. Chem. Soc.* **2006**, *128*, 15914.
- [22] J. X. Wang, S. Liang, H. Tan, Y. H. Wang, H. Y. Zang, Y. G. Li, *Chem. Select.* **2020**, *5*, 5883.
- [23] X. Wang, W. Mao, Y. Song, F. Meng, X. Hu, B. Liu, Z. Su, *Inorg. Chem.* **2021**, *60*, 18912.
- [24] L. Cronin, A. Müller, *Chem. Soc. Rev.* **2012**, *41*, 7325.
- [25] Müller, A., Sarkar, S., Shah, S., Qaiser, N., Bögge, H., *Angew. Chem., Int. Ed.* **1999**, *38*, 3238.
- [26] K. Tandekar, C. Singh, S. Supriya, *Eur. J. Inorg. Chem.* **2021**, *2021*, 734.
- [27] A. Lavoisier, J. Dalton, *Coord. Chem. Rev.* **2001**, *222*, 193.
- [28] Z. Garazhian, A. Rezaeifard, M. Jafarpour, A. Farrokhi, *ACS Appl. Nano Mater.* **2019**, *3*, 648.
- [29] J. Li, J. Lou, Z. Wang, L. Wang, F. Liu, X. Pu, J. Hu, S. Wang, C. Zhao, *ACS Sustain. Chem. Eng.* **2020**, *8*, 5880.
- [30] C. Xia, J. Li, Z. Qian, F. Xu, Y. Li, S. Zhu, H. J. Qian, C. Zhao, Z. Y. Lu, B. Yang, *Small* **2023**, *19*, 2205291.
- [31] C. Ru, Y. Gu, H. Na, H. Li, C. Zhao, *ACS Appl. Mater. Interfaces* **2019**, *11*, 31899.
- [32] C. Ru, Z. Li, C. Zhao, Y. Duan, Z. Zhuang, F. Bu, H. Na, *ACS Appl. Mater. Interfaces* **2018**, *10*, 7963.
- [33] S. Zhai, Z. Lu, Y. Ai, X. Liu, Q. Wang, J. Lin, S. He, M. Tian, L. Chen, *J. Membr. Sci.* **2022**, *645*, 120214.
- [34] J. Xu, Z. Zhang, K. Yang, W. He, X. Yang, X. Du, L. Meng, P. Zhao, Z. Wang, *J. Membr. Sci.* **2020**, *596*, 117711.
- [35] H. Chen, S. Wang, F. Liu, D. Wang, J. Li, T. Mao, G. Liu, X. Wang, J. Xu, Z. Wang, *J. Membr. Sci.* **2020**, *596*, 117722.
- [36] J. Xu, Z. Zhang, K. Yang, H. Zhang, Z. Wang, *Renew. Energy* **2019**, *138*, 1104.
- [37] Y. Duan, C. Ru, J. Li, Y.-N. Sun, X. Pu, B. Liu, B. Pang, C. Zhao, *J. Membr. Sci.* **2022**, *641*, 119906.

- [38] Y. Wang, X. Ma, G. Li, H. Li, Q. Wang, W. Chen, P. Ma, S. Li, J. Niu, J. Wang, *Chem* **2022**, 28, 202200637.
- [39] Y. Zhou, S. Liu, X. Hu, Y. Ge, C. Shi, H. Wu, T. Zhou, Z. Li, J. Qiao, *Process Saf. Environ. Prot.* **2023**, 172, 48.
- [40] J. Long, X. Zhang, S. Zeng, T. Pei, H. Ma, X. Li, X. Meng, *Int. J. Hydrogen Energy* **2023**, 48, 2001.
- [41] K. Jiao, X. Li, *Progr. Energy Combust. Sci.* **2011**, 37, 221.
- [42] L. Liu, S. He, S. Zhang, M. Zhang, M. D. Guiver, N. Li, *ACS Appl. Mater. Interfaces* **2016**, 8, 4651.
- [43] F. M. Zhang, L. Z. Dong, J. S. Qin, W. Guan, J. Liu, S. L. Li, M. Lu, Y. Q. Lan, Z. M. Su, H. C. Zhou, *J. Am. Chem. Soc.* **2017**, 139, 6183.
- [44] G. Zhao, X. Xu, H. Zhao, L. Shi, X. Zhuang, B. Cheng, Y. Yin, *J. Membr. Sci.* **2020**, 601, 117914.
- [45] L. Ma, J. Xu, S. Han, M. Yang, Z. Wang, H. Ni, Y. Gui, *J. Polym. Res.* **2014**, 21, 551.
- [46] Y. Yin, T. Xu, X. Shen, H. Wu, Z. Jiang, *J. Membr. Sci.* **2014**, 469, 355.
- [47] A. Barjola, J. L. Reyes-Rodríguez, O. Solorza-Feria, E. Giménez, V. Compañ, *Ind. Eng. Chem. Res.* **2021**, 60, 9107.